Japanese Journal of Applied Physics **50** (2011) 06GK06 **REGULAR PAPER**
DOI: 10.1143/JJAP.50.06GK06

Highly Uniform Fabrication of Diffraction Gratings for Distributed Feedback Laser Diodes by Nanoimprint Lithography

Yukihiro Tsuji*, Masaki Yanagisawa, Hiroyuki Yoshinaga, Naoko Inoue, and Toshio Nomaguchi

Transmission Devices R&D Laboratories, Sumitomo Electric Industries, Ltd., Yokohama 244-8588, Japan

Received November 30, 2010; accepted March 2, 2011; published online June 20, 2011

We have used a nanoimprint technique to fabricate diffraction gratings of distributed feedback laser diodes (DFB LDs) used in optical communication. We have aimed to establish the fabrication process featuring the high reproducibility of the period and linewidth of grating corrugations, which leads to an increase in the production yield of DFB LDs. The combination of the reverse tone nanoimprint and optimized etching techniques has contributed to the improvement of the reproducibility. The variation in grating period has been less than 0.2 nm and the variation in linewidth has been less than 10 nm over the six wafers. The results of this study indicate that our fabrication process for the diffraction gratings utilizing the nanoimprint technique has a high potential for the fabrication of DFB LDs. © 2011 The Japan Society of Applied Physics

1. Introduction

With the explosive growth in information communication technology (e.g., Internet, cloud computing, mobile telecommunication, social networks, and video-on-demand services), the growth of network traffic has led to demand for faster and denser communication infrastructures including optical communication networks. Distributed feedback laser diodes (DFB LDs) for optical communication systems have the advantages of high selectivity and stability of wavelength; thus, they increase the efficiency of band width in optical networks.[1–3] Although they have mainly been used in long-range and gigabit network nodes, they are now increasingly required in short-distance and end-user fields because of the increasing network traffic. Thus, inexpensive DFB LDs are becoming increasingly necessary. In recent years, not only DFB LDs but also tunable laser diodes have been used in optical networks.[4–9] Conventional DFB LDs has a fixed wavelength. Wavelength division multiplexing (WDM) systems require a separate fixed-wavelength laser emission for each wavelength; thus dozens of wavelength transmission system features separate dozens of lasers per fiber, each laser tuned to a unique wavelength. If one tunable laser could replace an array of fixed-wavelength lasers, the resultant system would be inexpensive and more efficient. Because of the potential importance of these devices to the future of all-optical networks, the market for tunable lasers is expected to be robust.

DFB LDs with uniform-period gratings [Fig. 1(a)] have been widely used for optical networks. The characteristics of a DFB LD with uniform gratings depend on the grating phase at the cleaved facet.[10,11] The variations in these characteristics with the facet phase are a serious issue from the viewpoints of productivity and usability.[12–14] One of the most effective methods of reducing the dependence of these characteristics on the facet phase is to convert uniform gratings into phase-shifted gratings [Fig. 1(b)].[15] The design of phase-shifted gratings is essential for achieving a high yield for DFB LDs. In tunable laser diodes, unique grating structures not only phase-shifted gratings but also chirped gratings [Fig. 1(c)] are required.

In general, there are various methods for fabricating diffraction gratings, for example, interference exposure and electron beam lithography (EBL). Interference exposure cannot feasibly be used for fabricating phase-shifted and chirped gratings because it exclusively generates exposure patterns with a uniform bright-and-dark period. Although EBL has a sufficient resolution to be used for phase-shifted and chirped gratings, exceedingly expensive EBL systems are required for mass production with a sufficient throughput.[16–18]

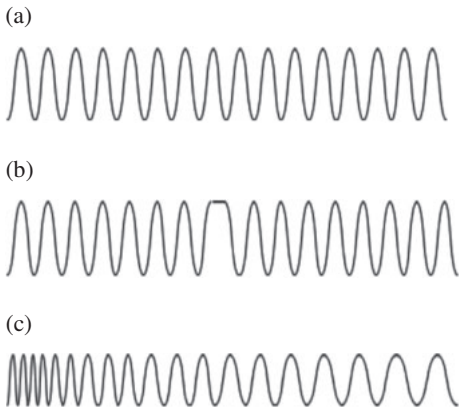

Fig. 1. Schematic structures of (a) uniform, (b) phase-shifted, and (c) chirped gratings.

Nanoimprint lithography (NIL) has been studied by many organizations since the middle of the 1990s. Chou *et al.* showed that sub-10-nm features could be formed by imprinting, which triggered the start of NIL technology.[19] A novel method of NIL using a UV-curable polymer was introduced by Haisma *et al.*[20]

We have employed the nanoimprint technique to form diffraction gratings of distributed feedback laser diodes (DFB LDs) with a wavelength of 1300 or 1500 nm for optical communication.[21–23] The linewidth of diffraction gratings is a critical factor of DFB LDs, because it significantly affects the coupling coefficient. Compound semiconductor substrates, such as InP, used for the fabrication of DFB LDs have a certain undulation, which deteriorates the uniformity of the linewidth of the imprinted resin. Thus, we have applied a reverse tone nanoimprint process to the fabrication of the gratings in order to improve the uniformity across a wafer.

In this study, we have optimized that the uniformities of linewidth and the period of the gratings to manufacture

*E-mail address: tsuji-yukihiro@sei.co.jp

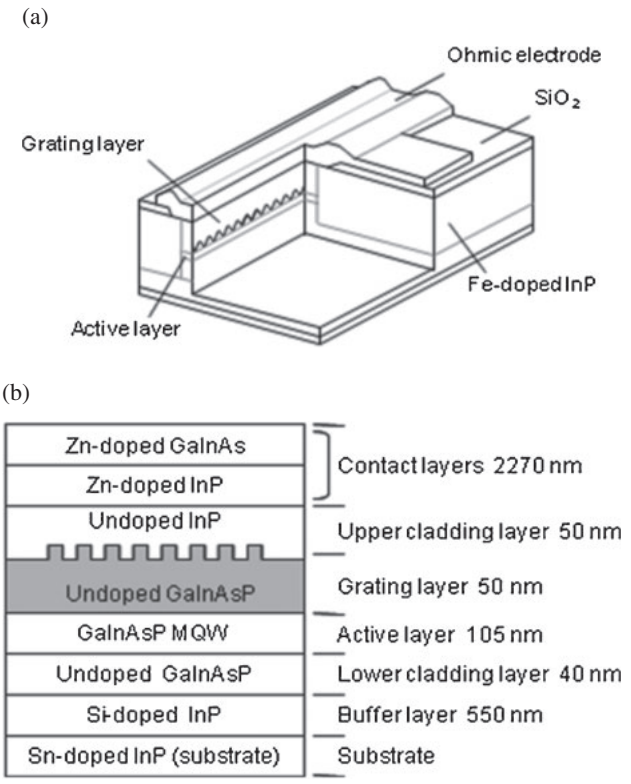

Fig. 2. Schematic structures of (a) the DFB LD and (b) its epitaxial layers.

diffraction gratings of DFB LDs. We have evaluated the uniformities of characteristics in order to evaluate the feasibility of the process as a manufacturing method.

2. Experimental Procedure

Schematic structures of the LD and its epitaxial layers are shown in Figs. 2(a) and 2(b), respectively. We have prepared a 2-in.-diameter InP substrate with epitaxial layers including an active layer, a grating layer, and a lower cladding layer grown by metalorganic vapor phase epitaxy (MOVPE). The reverse tone nanoimprint process is shown in Fig. 3. Grating patterns using a quartz mold have been transferred on the wafers by a serial process described below.

First, we deposit a silicon nitride (SiN) film with a thickness of 40 nm on the epitaxial wafer by plasma-enhanced chemical vapor deposition. Second, an 80-nm-thick film of primer material as an adhesion layer is spin-coated between the SiN film and the UV-curable resin [Fig. 3(a)]. Third, a quartz mold with a size of $8 \times 6\,\mathrm{mm}^2$ is pressed on a dispensed UV curing resin at a force of 4 N in 16 fields on the wafer by a step and repeat process [Fig. 3(b)]. Fourth, the spin coating of a 200-nm-thick silicon-containing resin is followed by etch back by reactive ion etching (RIE) to reveal the top of the imprinted feature [Figs. 3(c) and 3(d)], which is etched through the wafer by inductively coupled plasma RIE (ICP-RIE) using oxygen as the etching gas [Fig. 3(e)]. Fifth, the revealed layer is selectively etched by RIE until the SiN masks are revealed [Fig. 3(f)]. Sixth, the grating patterns of the SiN film and resin layers are removed by O_2 ashing. Last, we use ICP-RIE

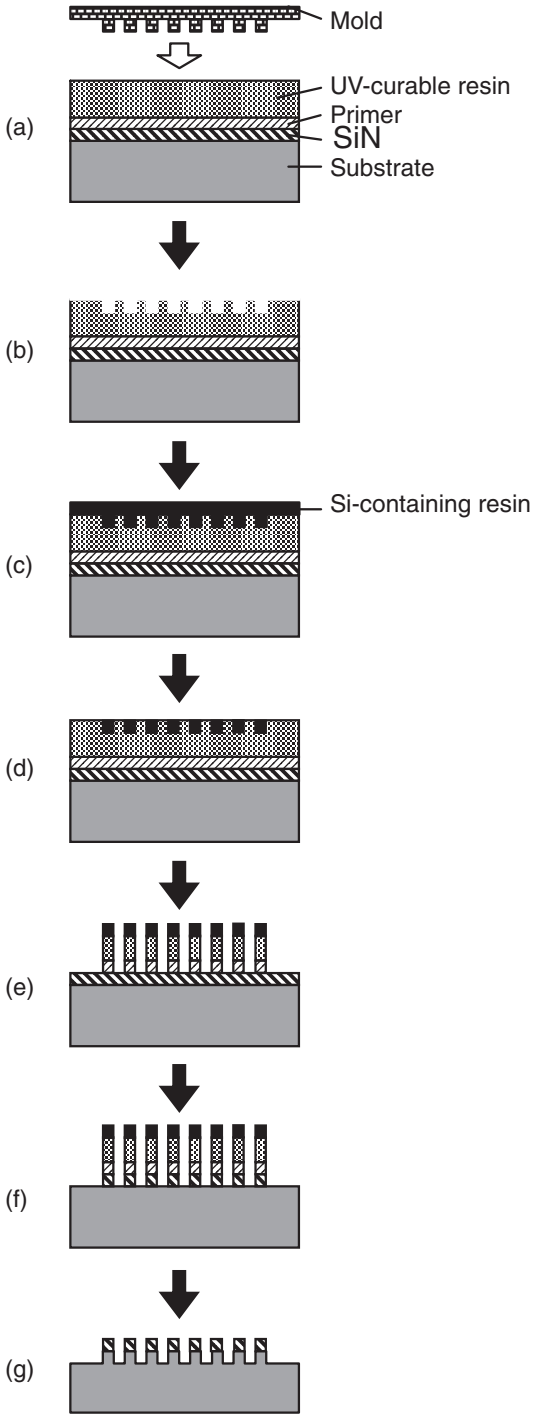

Fig. 3. Fabrication process for the diffraction gratings.

with CH_4/H_2 gas for the etching of the epitaxial layer [Fig. 3(g)].

After the formation of diffraction gratings, an upper cladding layer and contact layers are formed on the grating layer by MOVPE. The contact layers consist of InP and GaInAs layers [Fig. 2(b)]. Then, stripe patterns of SiO_2 are formed on the contact layers to define the cavities of the LDs. The stripe patterns are used as masks for subsequent crystal etching by ICP-RIE with CH_4/H_2 as the etching gas. Then, Fe-doped InP is selectively grown as an insulating layer by MOVPE. Subsequently, a SiO_2 film is deposited as a passivation layer, in which contact holes are formed by selective etching by RIE. Finally, metal electrodes are

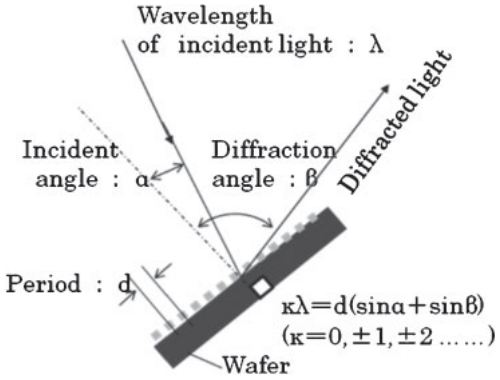

Fig. 4. Measurement method for diffraction angle.

formed by high-vacuum evaporation and the lift-off method. In this study, we used a mold with grating periods of 195 and 202 nm because we aimed to fabricate DFB LDs with the wavelengths of 1265 and 1305 nm. Here, the linewidth is approximately 140 nm and the space width is approximately 60 nm.

We have improved the condition of the break-through etching using the ICP-RIE system. The etching rate of the adhesion layer is 200 nm/min and the etching selectivity ratio is more than 30. The etching time is 3 min. We used a mixture of oxygen and nitrogen or CF_4 as the etching gas. The linewidths of the fabricated patterns are measured by scanning electron microscopy (SEM) after O_2 ashing.

We evaluated the wafer-to-wafer uniformities of the linewidth and period of the gratings by a method described below. A schematic diagram of the experimental setup used is shown in Fig. 4. This setup consists of incident light, a detector, and a wafer stage with a built-in goniometer. The wavelength of the incident light is 364.8 nm. By using the mold, we formed diffraction gratings with the corresponding eight periods: 194.1, 194.7, 195.3, 195.9, 196.5, 201.4, 202.6, and 203.8 nm. We also measured the diffraction angle of the gratings using this setup and calculated the period of the gratings using Bragg's law.

3. Results and Discussion

Figure 5(a) shows the SEM image of the grating pattern with undercut after break-through etching using conventional conditions, which were a bias power of 100 W and a mixture of oxygen and CF_4 as the etching gas, whose flow rates were 4 and 6 sccm, respectively, when the substrate temperature was uncontrolled. Figure 5(b) shows the SEM image of the grating pattern achieved by using improved conditions, which were a bias/ICP power of 70 W/250 W and a mixture of oxygen and nitrogen as the etching gas, whose flow rates were 1 and 9 sccm, respectively, when the substrate was at a temperature of $-10\,^{\circ}C$.[24,25] It is considered that the vertical shape is achieved by the optimized plasma density and sidewall effect[26] by the etching gas, and the optimized substrate temperature.[27] In general, the large undercut of the line pattern is frequently found in the resin etching process [Fig. 5(c)]. However, no significant undercut has been found in the grating pattern fabricated by the optimized etching conditions developed in this study. We consider that the undercut is reduced by the deposition of what on the

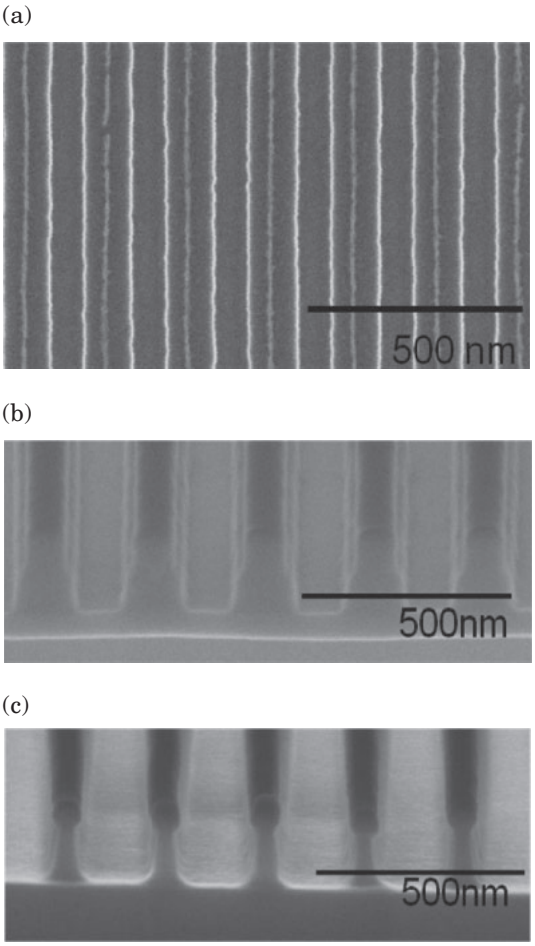

Fig. 5. Scanning electron microscopy images of (a) top view and (b) before and (c) after improvement of the grating pattern.

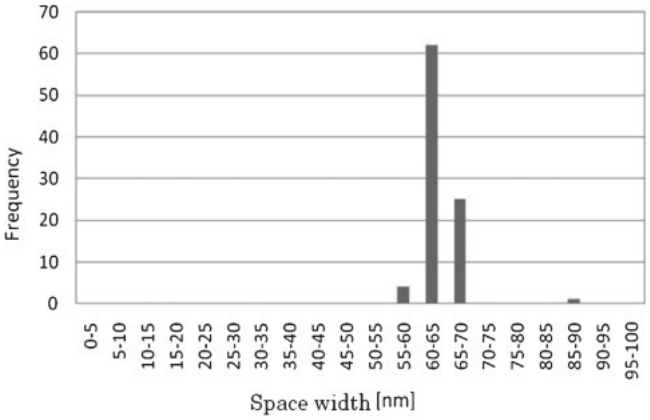

Fig. 6. Histogram of space width in six wafers including 96 fields.

sidewall, which consists of carbon nitride generated from the imprinted resin and nitrogen as the etching gas.[28–30]

We have evaluated the wafer-to-wafer uniformity of the linewidth. Figure 6 shows the histogram of the space width within six wafers. The variation in space width is less than 10 nm in 3σ. We consider that the uniformity of space width is improved by reducing the undercut in the break-through etching process.[31–33]

The diffraction light of the grating pattern transferred from the period-measuring mold is shown in Fig. 7.

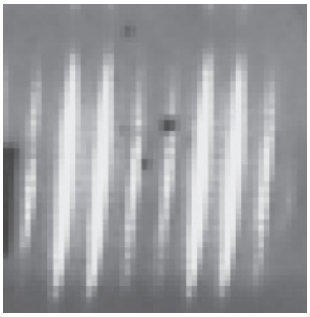

Fig. 7. Image of diffracted light.

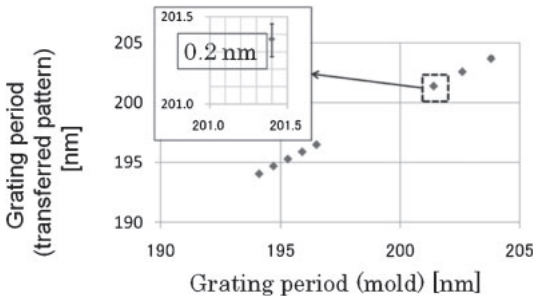

Fig. 8. Correlation diagram of grating period within six wafers.

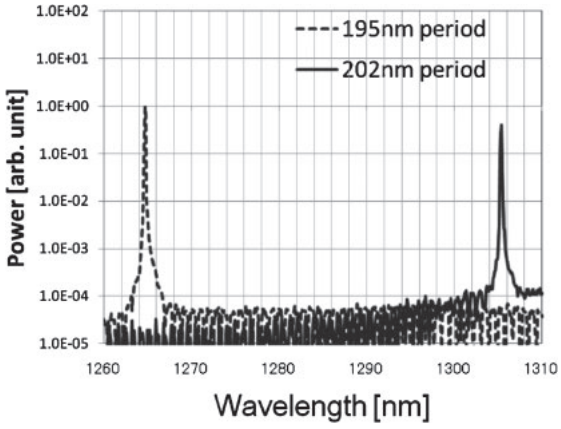

Fig. 9. Oscillation spectrum of a phase-shifted LD.

Therefore, the angle of the diffraction light corresponds to the period of the diffraction grating. Figure 8 shows a correlation between the measured and designed grating periods and the variation in measured grating period within six wafers. The variation in grating period is less than 0.2 nm, indicating that the diffraction grating of the mold is transferred to the wafers efficiently. We have also succeeded in the fabrication of the diffraction gratings with various periods by using one mold.

The oscillation spectrum of the phase-shifted DFB LD is shown in Fig. 9. It indicates that the DFB LDs with grating periods of 195 and 202 nm shows intensity peaks at 1265 and 1305 nm, respectively. It is considered that each DFB LD oscillated at the designed Bragg wavelength.

We compared the side-mode suppression ratio (SMSR)[34] of phase-shifted DFB LDs fabricated by NIL with that of

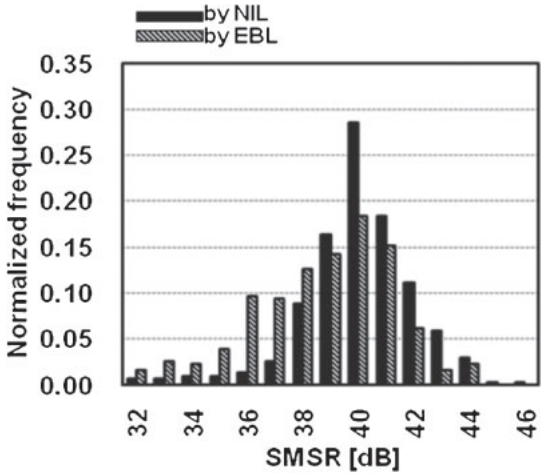

Fig. 10. Histograms of SMSR for phase-shifted LDs fabricated by NIL and EBL.

phase-shifted DFB LDs fabricated by EBL. The SMSR is one of the parameters that indicate the stability of the single-mode emission of DFB LDs. Transmitters for optical communication systems are typically required to have an SMSR of more than 40 dB. Lower SMSRs may lead to intolerable intensity noise through mode partition noise or to large levels of crosstalk in WDM systems. The SMSR is determined by the ratio of the main peak power to the second one in the oscillation spectrum. The histograms of SMSR for both types of DFB LD, which are shown in Fig. 10, indicate comparable variations in SMSR.

4. Conclusions

We applied a reverse tone nanoimprint process to the fabrication of diffraction gratings for DFB LDs. We improved the "across wafer" and "wafer-to-wafer" uniformities of linewidth by reducing under-cut in the break-through etching process. The results showed that the linewidth uniformity (3σ) was less than 10 nm in six wafers including 96 imprint fields. The grating period range over six wafers was less than 0.2 nm. The diffraction grating periods of the mold were transferred to the wafers efficiently.

We successfully demonstrated the fabrication of phase-shifted DFB LDs by NIL, which have comparable characteristics to those fabricated by EBL. The DFB LDs showed oscillation wavelengths that corresponded to the designed Bragg wavelength, indicating that the diffraction grating period of the mold was transferred to LDs by NIL efficiently.

The results of this study indicate that our fabrication process for the diffraction gratings utilizing a nanoimprint technique has a high potential for the fabrication of DFB LDs.

1) H. Kogelnic and C. V. Shank: Appl. Phys. Lett. **18** (1971) 152.
2) K. Utaka, S. Akiba, K. Sakai, and Y. Matsumura: Electron. Lett. **17** (1981) 961.
3) T. Matsuoka, H. Nagai, Y. Itaya, Y. Noguchi, Y. Suzuki, and T. Ikegami: Electron. Lett. **18** (1982) 27.
4) R. C. Alferness, U. Koren, L. L. Buhl, B. I. Miller, M. G. Young, T. L. Koch, G. Raybon, and C. A. Burrus: Appl. Phys. Lett. **60** (1992) 3209.

5) V. Jayaraman, L. A. Cohen, and L. A. Coldren: Proc. Optical Fiber Communication Conf. Expo., 1992, WL12.
6) W. Idler, M. Schilling, D. Baums, G. Laube, K. Wunstel, and O. Heldebrand: Electron. Lett. **27** (1991) 2268.
7) Y. Yoshikuni, Y. Tohmori, T. Tamamura, H. Ishii, Y. Kondo, M. Yamamoto, and F. Kano: Proc. Optical Fiber Communication Conf. Expo., 1993, TuC2.
8) Y. Tohmori, Y. Yoshikuni, H. Ishii, F. Kano, T. Tamamura, Y. Kondo, and M. Yamamoto: IEEE J. Quantum Electron. **29** (1993) 1817.
9) M. Seki, C. Fukuda, K. Fujii, K. Koyama, K. Hiratsuka, M. Murata, and T. Kato: Ext. Abstr. (57th Spring Meet., 2010); Japan Society of Applied Physics and Related Societies, 19p-E-9 [in Japanese].
10) T. Matsuoka, H. Nagai, Y. Noguchi, Y. Suzuki, and Y. Kawaguchi: Jpn. J. Appl. Phys. **23** (1984) L138.
11) M. Davis and R. O'Dowd: IEEE. J. Quantum Electron. **30** (1994) 2458.
12) W. Streifer, R. D. Burnham, and D. R. Scifres: IEEE J. Quantum Electron. **11** (1975) 154.
13) T. Matsuoka, Y. Yoshikuni, and H. Nagai: IEEE J. Quantum Electron. **21** (1985) 1880.
14) D. C. Franders, H. Kogelnik, R. V. Schmidt, and C. V. Shank: Appl. Phys. Lett. **24** (1974) 194.
15) C. Kaden, U. Griesinger, H. Schweitzer, M. H. Pilkuhn, and N. Stath: J. Vac. Sci. Technol. B **10** (1992) 2970.
16) K. Sekartedjo, N. Eda, K. Furuya, Y. Suematsu, F. Koyama, and T. Tanbun-Ek: Electron. Lett. **20** (1984) 80.
17) H. Yagi, T. Sano, K. Ohira, D. Plumwongrot, T. Maruyama, A. Haque, S. Tamura, and S. Arai: Jpn. J. Appl. Phys. **43** (2004) 3401.
18) H. Yagi, Y. Ohnishi, K. Koyama, Y. Tsuji, H. Ichikawa, H. Yoshinaga, H. Kaida, T. Nomaguchi, K. Hiratsuka, and K. Uesaka: SEI Tech. Rev. **175** (2009) 120 [in Japanese].
19) S. Y. Chou, P. R. Krauss, and P. J. Renstrom: Appl. Phys. Lett. **67** (1995) 3114.
20) J. Haisma, M. Verheijen, K. Heuvel, and J. Berg: J. Vac. Sci. Technol. B **14** (1996) 4124.
21) M. Yanagisawa, Y. Tsuji, H. Yoshinaga, N. Kono, and K. Hiratsuka: Jpn. J. Appl. Phys. **48** (2009) 06FH11.
22) M. Yanagisawa, Y. Tsuji, H. Yoshinaga, K. Hiratsuka, and J. Taniguchi: J. Phys.: Conf. Ser. **191** (2009) 012007.
23) M. Yanagisawa, Y. Tsuji, H. Yoshinaga, N. Kono, and K. Hiratsuka: SEI Tech. Rev. **177** (2010) 69 [in Japanese].
24) Y. Tsuji, M. Yanagisawa, H. Yoshinaga, and K. Hiratsuka: J. Phys.: Conf. Ser. **191** (2009) 012010.
25) K. Tsujimoto, S. Okudaira, and S. Tachi: Jpn. J. Appl. Phys. **30** (1991) 3319.
26) T. Kure, H. Kawakami, S. Tachi, and H. Enami: Jpn. J. Appl. Phys. **30** (1991) 1562.
27) H. Kinoshita, A. Yamauchi, and M. Sawai: Tech. Rep. IEICE SDM94-114 (1994) [in Japanese].
28) Y. Kimura, R. Aoyama, S. Suzuki, and H. Ohtsuka: Proc. SPIE **1803** (1992) 107.
29) H. Kinoshita and A. Yamauchi: Proc. 2nd Int. Conf. Reactive Plasmas, 1994, p. 459.
30) Y. Kimura, R. Aoyama, and S. Suzuki: Proc. 2nd Int. Conf. Reactive Plasmas, 1994, p. 455.
31) Y. Tsuji, M. Yanagisawa, H. Yoshinaga, K. Ishihara, and K. Hiratsuka: Ext. Abstr. (56th Spring Meet., 2009); Japan Society of Applied Physics and Related Societies, 30p-K-10 [in Japanese].
32) Y. Tsuji, H. Yoshinaga, M. Yanagisawa, K. Hiratsuka, and T. Nomaguchi: Ext. Abstr. (70th Autumn Meet., 2009); Japan Society of Applied Physics, 9a-D-10 [in Japanese].
33) Y. Tsuji, H. Yoshinaga, N. Inoue, M. Yanagisawa, and T. Nomaguchi: Ext. Abstr. (71th Autumn Meet., 2010); Japan Society of Applied Physics, 15a-K-7 [in Japanese].
34) B. Moeyersoon, S. Member, G. Morthier, and M. Zhao: IEEE J. Quantum Electron. **40** (2004) 241.